

Design, path planning improvement and test of a portable massage robot on human back

Wendong Wang¹, Peng Zhang, Chaohong Liang and Yikai Shi

Abstract

A massage robot that helps to improve the quality of human life has attracted more interests of researchers and consumers. A portable back massage robot that is compact and space-saving was designed to be used on human back instead of a traditional large-scale structure robot. To design the massage robot, the models of electric circuit, magnetic circuit and mechanics were analyzed to achieve optimal massage force. Parameters of the massage actuator are determined based on the influence analysis of the coil current, the coil turns and the distance between the moving core and the yoke on the electromagnetic force. The massage coverage of human back, which is used to calculate the massage effect, could be improved by an excellent path planning algorithm. This article proposed an efficient full covered path planning algorithm for the designed massage robot, and the relevant algorithm models were established. Simulation results show that the coil current is much more sensitive to electromagnetic force of the moving core compared to the other two factors, and the presented path planning algorithm completes full coverage of the massage robot on the back area. The experimental platform of the massage robot was built, and the influence of the input signal duty cycle, the input signal voltage and the hardness of the massage object on the massage effect was discussed by testing the values of acceleration. The tested results show that the massage effect is best when the duty cycle is in the range of 1/8–1/2. Meanwhile, the hardness of massage parts affects the massage intensity. The consistency between the tested results of path planning and simulation verifies the feasibility of the simulation procedure and indicates that the massage robot can attain the desired massage performance and realize the planned paths.

Keywords

Portable massage robot, path planning, electromagnetic force, coverage of massage area, traditional Chinese medicine

Date received: 25 January 2018; accepted: 10 June 2018

Topic: Medical Robotics

Topic Editor: Marco Ceccarelli

Associate Editor: Jorge Solis

Introduction

An intelligent massage robot is desirable for improving the quality of human life based on traditional Chinese medicine (TCM) that is considered an effective physiological treatment to improve blood circulation, relieve fatigue and reduce muscle pain.^{1,2} There has been a remarkable growth in the usage of massage manipulators since the past decade, prominent among them being massage chairs, massage hammer, massage cape and massage bots.³ However, these

School of Mechanical Engineering, Northwestern Polytechnical University, Xi'an, Shaanxi, China

Corresponding author:

Wendong Wang, School of Mechanical Engineering, Northwestern Polytechnical University, Xi'an, Shaanxi 710072, China.

Email: wdwang@nwpu.edu.cn



Creative Commons CC BY: This article is distributed under the terms of the Creative Commons Attribution 4.0 License (<http://www.creativecommons.org/licenses/by/4.0/>) which permits any use, reproduction and distribution of the work without further permission provided the original work is attributed as specified on the SAGE and Open Access pages (<https://us.sagepub.com/en-us/nam/open-access-at-sage>).

massage products are usually unsatisfactory for their functional insufficiency of intelligence and safety.⁴ More and more researchers devote to develop high intelligent massage equipment or robot to prompt the product's functionality in safety, path planning and massage effect.⁵⁻⁷

A passivity-based impedance controller was used to develop a 4-degree of freedom (DOF) anthropomorphic robotic arm with integrated elastic joints to reproduce the manipulation of TCM remedial massage and meanwhile guarantee safety proposed by Huang et al.⁸ A path generator control system and virtual compliance calculator were developed for maxillofacial massage robots with 6-DOF by Ishii et al.⁹ Luo and Hsieh¹⁰ implemented the tapping motion with a dual arm robot based on the impedance control, and the results show that it can effectively imitate the tapping motion of massage therapists. A massage robot was developed based on the clinical requirements of TCM massage and healthcare for rehabilitation for chronic disease by Gao et al.¹¹ There are also some massage robots that were developed for specific body parts, such as oral (facial) tissues,^{12,13} chest (back)¹⁴ and feet.¹⁵ From the analysis of the state of the art, although existing robots could provide more functions and become more intelligent, they are still difficult to be widely spread due to the complexity of the control system, high cost and heavy structure.¹⁶ Moreover, all the above-mentioned researchers focus on large-scale structure massage robots located in hospitals or rehabilitation centers,¹⁴ and some of which were directly developed from industrial robots used as a base for half-autonomous or autonomous massage robots. The intelligent massage robot that is conveniently used at home is merely mentioned. In addition, in case of human back movements, the existing programmed motion planning of the massage robot is not suitable.

Consequently, to overcome the existing problems of the massage robot in control, structure and coverage of path planning, this article aims to develop a novel portable massage robot that successfully completes tapping, kneading and rolling operation on human back. Different from existing large-scale structure massage robots, our robot could easily be used at home for its compact and space-saving structure. Furthermore, an efficiently full covered path planning algorithm was specifically proposed to increase massage coverage such that the massage effect is improved.

Design of the massage robot

Analysis of the massage robot actuator

The massage head model consists of electric circuit, magnetic circuit and mechanics that are explained as follows.

The coil and the moving core can be described as the electric circuit model, and the driving voltage is

$$u = Ri + \frac{d\psi}{dt} = Ri + \frac{dLi}{dt} \quad (1)$$

The equivalent coil inductance is

$$L = \frac{N^2}{R_m + R_\delta + R_l} \quad (2)$$

where R is the equivalent resistance, i is the coil current, ψ is the flux linkage generated by the coil in the magnetic field, N is the coil turn's number, R_m is the equivalent magnetic reluctance, R_δ is the equivalent working air-gap reluctance and R_l is the equivalent nonworking air-gap reluctance.

To simplify analysis, it is assumed that the coil inductance L does not change during movement, so equation (1) can be simplified as

$$u = Ri + L \frac{di}{dt} \quad (3)$$

To solve equation (3), when the massage head is powered on, the coil current is calculated as

$$i = i_0 e^{-\frac{t}{\tau}} + \frac{u}{R} \left(1 - e^{-\frac{t}{\tau}} \right) \quad (4)$$

where $\tau = L/R$ and i_0 is current initial value.

When the moving iron core is magnetized, the magnetic circuit model is

$$\begin{aligned} iN &= \Phi(R_m + R_\delta + R_l) \\ B &= \frac{iN}{AR_\delta} \\ R_\delta &= \frac{l_\delta}{\mu_0 A} \\ F_m &= \frac{\mu_0 i^2 N^2 A}{2(\delta - x)^2} \end{aligned} \quad (5)$$

where Φ is the magnetic stroke flux, A is the area of electromagnetic action, δ is the initial stroke, μ_0 is the air permeability, x is the displacement of moving core ($0 \leq x \leq \delta$) and F_m is the electromagnetic force of moving iron core.

The magnetic moving iron core is knocked down with electromagnetic force and the motion equation is expressed as

$$m \frac{dv}{dt} = F_m - F_f - F_k \quad (6)$$

where m is the mass of the magnetic moving iron core and v is the velocity.

Based on equations (5) and (6), the motion differential equation is obtained as

$$m\ddot{x} = \frac{\mu_0}{2} \cdot \frac{i^2 N^2 A}{(\delta - x)^2} - F_f - kx \quad (7)$$

where F_k is the spring load and F_f is the back resistance of human body ($F_f = 0$ when the moving iron core moves from the initial position to contact back).

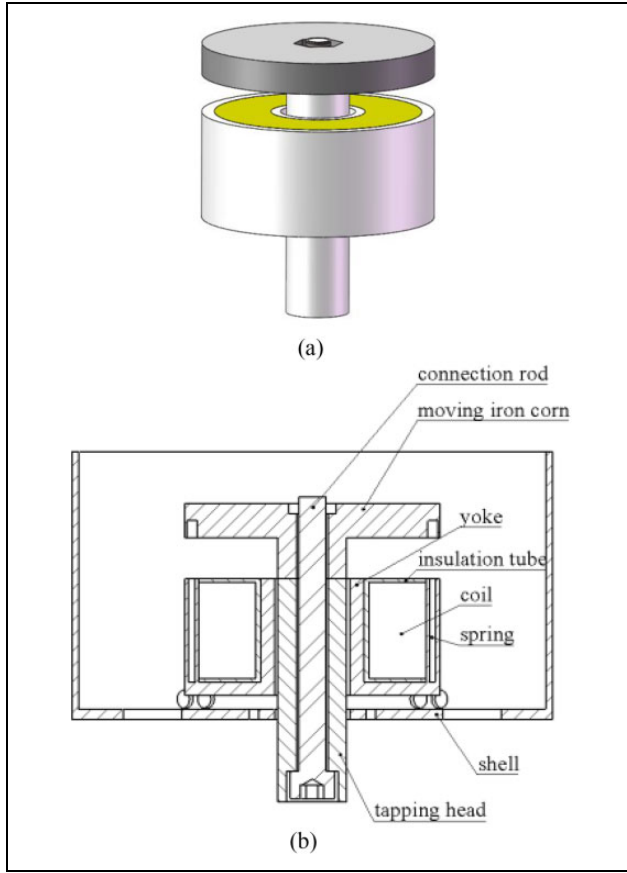


Figure 1. The 3D model of the massage actuator. (a) 3D model. (b) Section view. 3D: three-dimensional.

Based on the above analysis, it can be concluded that the factors affecting the dynamic characteristics of the massage head include coil voltage (current), the number of turns of the coil, the distance of moving iron core and yoke, the equivalent mass of moving iron core and the connected massage head, the elastic coefficient of spring and the magnetic materials. The final design result of the massage actuator is shown in Figure 1.

3D model of the massage robot

The characteristics of TCM massage techniques were analyzed considering back massage environment, and finally three kinds of massage operations were determined, namely tapping, rolling and kneading. In order to achieve these three massage operations, massage head was designed to achieve tapping operation based on the principle of electromagnetic induction, the use of roller and control algorithm to achieve rolling and kneading operation, and ultimately the three-dimensional (3D) model of the massage robot structure is designed as shown in Figure 2.

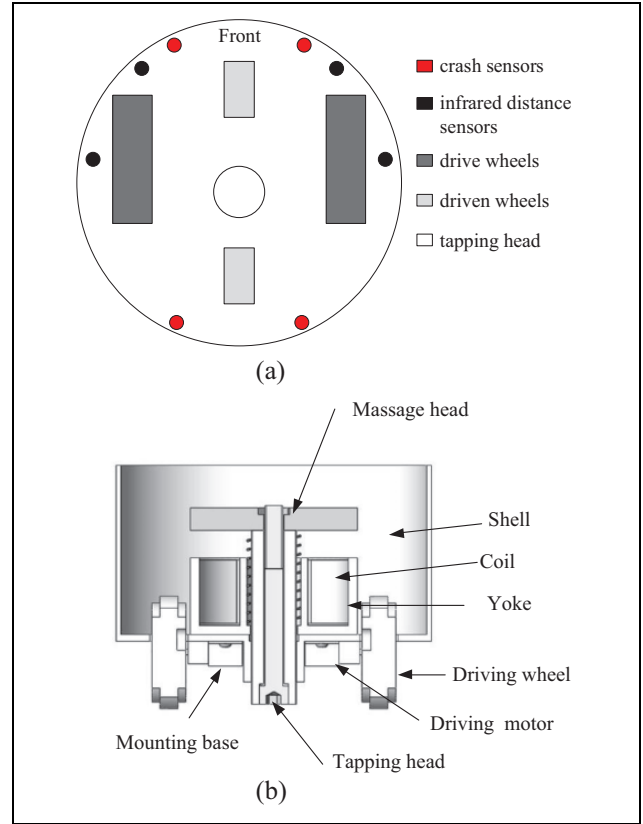


Figure 2. The 3D model of the massage robot. (a) The top view. (b) The section view. 3D: three-dimensional.

Table 1. The weight and dimension of the main parts.

Name	Dimension (mm)		Weight (kg)
Shell	Diameter	140	0.35
	Height	78	
Coil	Diameter	66	0.88
	Height	35	
Tapping head	Diameter	18	0.40
	Height	65	
Driving wheel	Diameter	50	0.22
	Width	15	

The main parameters of the designed massage robot are listed in Table 1.

The working principle of the massage head is described as follows: the winding coil is placed around the yoke, and when the winding coil is energized, the moving iron core is magnetized and linearly moves under the action of the electromagnetic force. When the power of the coil is cut off, the electromagnetic force disappears and the moving iron core returns back to the original position with the spring force. When the coil is de-energized periodically, it can be achieved in the moving iron core periodically tapping.

Table 2. Average and deviation of all these factors.

Factors	Average			Deviation
A	A ₁	A ₂	A ₃	0.0179
	4.16	4.65	5.03	
B	B ₁	B ₂	B ₃	0.0461
	3.91	4.62	5.31	
C	C ₁	C ₂	C ₃	0.0153
	5.04	4.55	4.24	

Model calculation

The 3D electromagnetic simulation model of the massage head was established in Maxwell. In order to investigate the influence and the relationship between the influence factors that affect electromagnetic force, the orthogonal design method was used to analyze the sensitivity,¹⁷ and the electromagnetic force was calculated. By analyzing the results, the main factors that affect the tapping force can be determined by the minimum number of calculations.

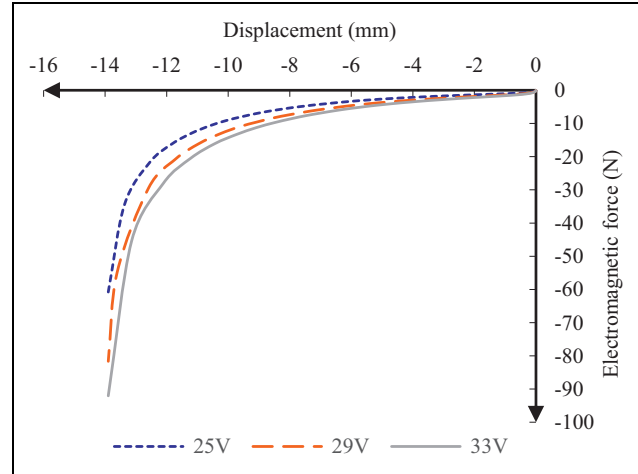
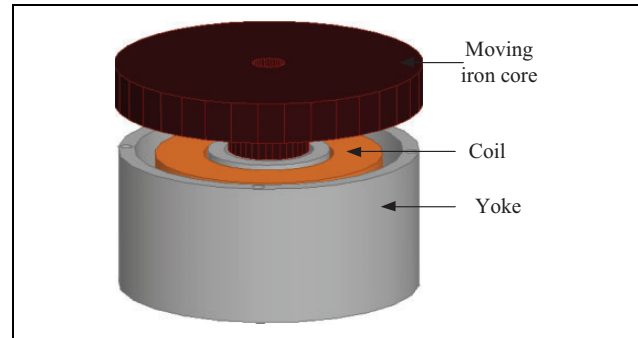
The materials and geometrical parameters of the massage head were determined by the design requirements, thereby its impact on electromagnetic force was not considered. The following factors were chosen to discuss the impact, the number of coil turns (N , factor A), coil voltage (V , factor B) and the distance between the moving core and the yoke (mm, factor C).

In our previous work, the three factors have been calculated with the aforementioned method in Maxwell and MATLAB. The simulation results were obtained (see Table 2) to analyze the difference and influence on massage operation, and the calculation shows the coil voltage is much more sensitive to electromagnetic force compared to other two factors.¹⁸

Optimization of massage head and its intensity control

With the above analysis and the previous achievements, considering the massage comfort and simulation of electromagnetic force and other factors, this article determines the distance between the moving iron core of massage head and the yoke is 14 mm; considering the size of the yoke, coil diameter and other factors, the number of coil turns is set as 2100. When the coil voltage is 25, 29 and 33 V, the displacements of the moving core and the electromagnetic force are shown in Figure 3.

It can be seen that the electromagnetic force is from 8 N to 40 N during the massage head tapping the back (10–14 mm) when the coil voltage is 25 V; it is 11–60 N when the coil voltage is 29 V and it is 12–90 N when the coil voltage is 33 V. This calculation was obtained without considering the magnetic flux leakage. Due to the difference of the magnetic circuit structure, the massage strength is less than 30 N under the spring resistance and the viscoelastic resistance of the human back. According to our previous massage experience, the intensity can be 8–30 N when tapping

**Figure 3.** Electromagnetic force variation with displacement of moving iron core.**Figure 4.** 3D simulation model of massage head. 3D: three-dimensional.

the back, so the experimental tapping force meets the massage requirements.

The 3D model of the simplified massage head, as shown in Figure 4, was built to perform electromagnetic simulation in Maxwell. The simulation results show that when the coil voltage is 33 V at 65 ms, the massage head completes the pull action, and the vector distribution of the magnetic flux density B of the moving iron core is depicted in Figure 5(a). It indicates that the total magnetic flux of the inner and outer ring is the same. The reason is the structure design of the yoke ensures the same volume of the inner and outer ring, which creates the same B (0.7 T). From Figure 5(b), it denotes the distribution of B is non-linear. This distribution is consistent with the distribution of magnetic induction in the yoke.

Analysis and simulation of path planning algorithm

Efficient full coverage path planning algorithm

The presented portable massage robot is a typical mobile robot whose target position has to be reached without

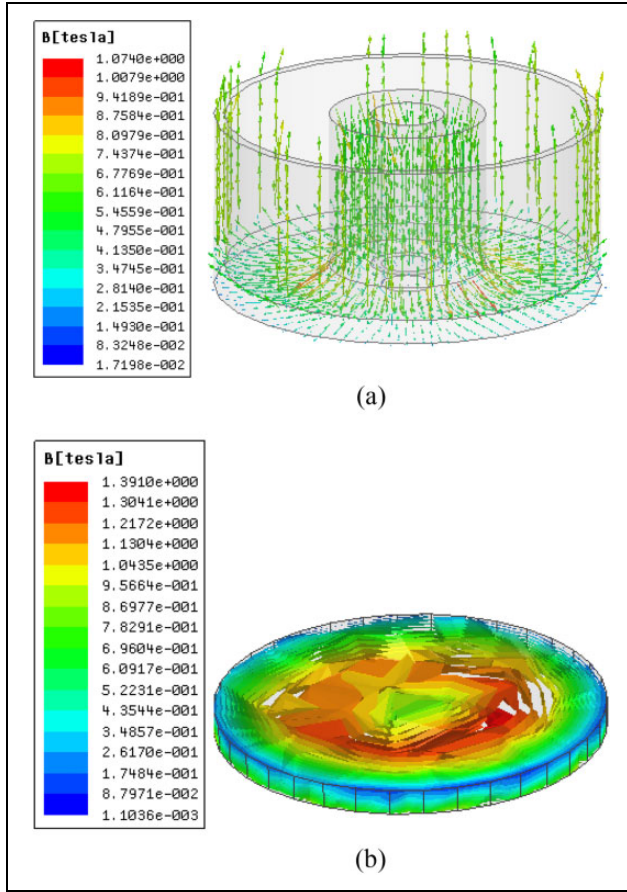


Figure 5. Distribution of magnetic flux density B at 65 ms. (a) B of yoke vector distribution. (b) B of moving iron core scalar distribution.

colliding with obstacles during movement. Path planning approaches of a mobile robot have been widely investigated to improve coverage.¹⁹ An efficient online approach for complete coverage path planning of mobile robots in an unknown workspace was proposed based on boustrophedon motion and an optimized backtracking mechanism.²⁰ Different from service or medical robots, the movement environment and path planning object in this article changes to a portable mobile robot working on human back.^{21,22} Therefore, the existing path planning algorithms are not applicable for the object of the article.

In order to achieve full coverage of the massage area, it requires the massage robot to move in accordance with a trajectory in the entire area. According to the design targets, the presented massage robot needs to complete both tapping path and rolling (kneading) path. The tapping path is the massage path that uses the massage head by the electromagnetic induction and the rolling (kneading) path is the movement path by two driving wheels. After analysis and discussion, when using the boustrophedon path planning algorithm along the back of the human body to massage, the robot could

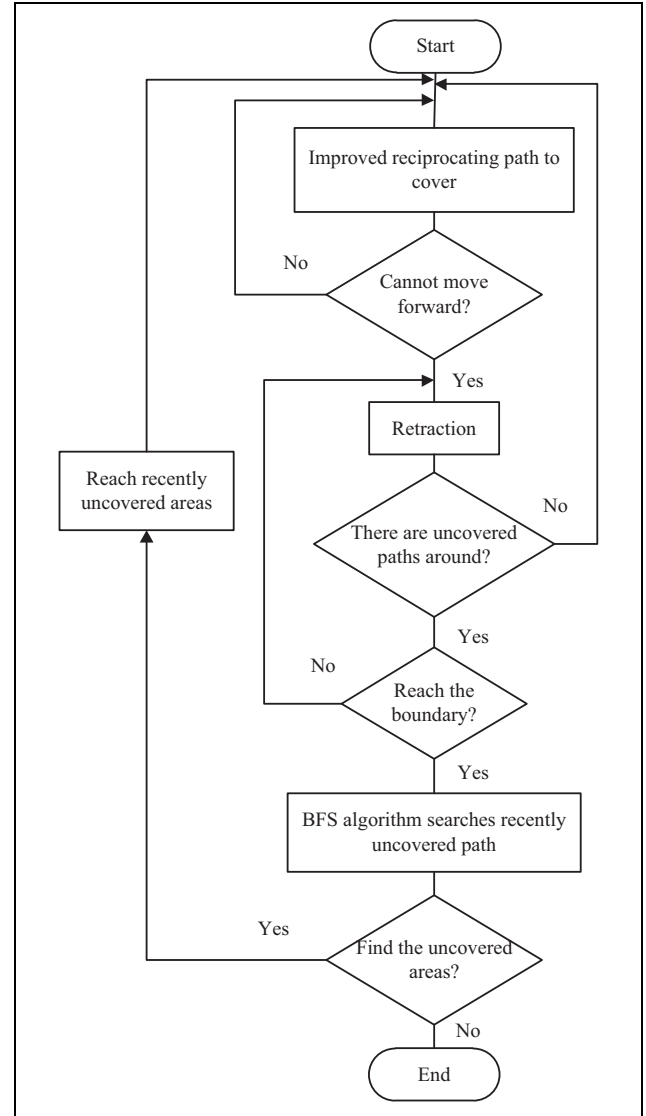


Figure 6. Effective full covered path planning algorithm flow chart.

only effectively cover one-third or two-thirds of the entire massage area.²³ To further increase the regional coverage and improve the massage effect, this article proposes an efficient full coverage path planning algorithm based on the traditional boustrophedon path planning algorithm.

The flow chart representing the proposed improved algorithm is shown in Figure 6. An improved boustrophedon path planning algorithm is firstly used when starting the programme. All past areas could be marked by the algorithm. If the front edge or obstacle is encountered in the front, the retraction method is adopted. Otherwise, the breadth-first search (BFS) algorithm is used to search for a nearby unoccupied area until all planning areas are marked.²⁴ In addition, the improved boustrophedon algorithm is obtained once the traditional boustrophedon algorithm overlaps the first coverage path.

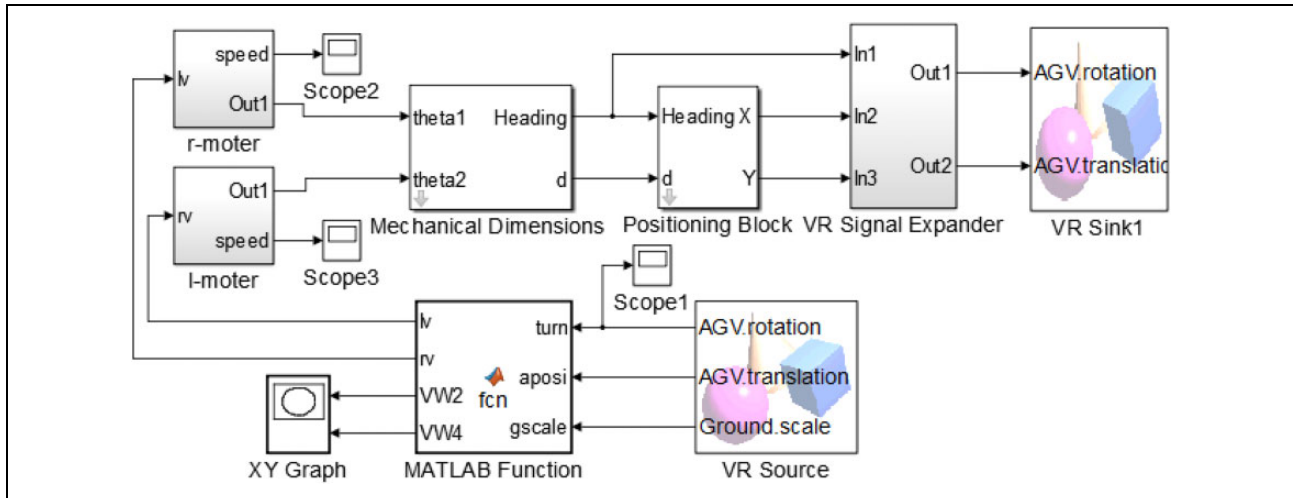


Figure 7. Control system model of massage robot.

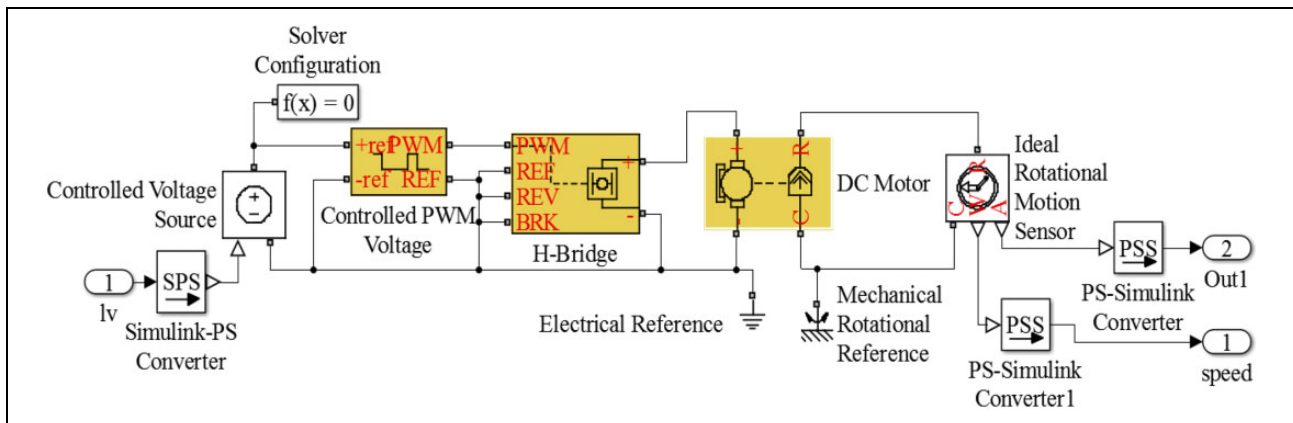


Figure 8. Control subsystem model of motor drive.

Control system modelling

In this article, the Simulink model of the wheeled massage robot control system includes a control subsystem of the motor, path algorithm control subsystem, parameter module of the massage robot and virtual reality (VR) interface module (see Figure 7). The control signal is directly outputted to a virtual operating environment by the VR Sink block, and the operation of the massage robot could be visualized through a browser window. As shown in Figure 8, the DC geared motor is selected to drive the control subsystem, which includes PWM wave generator and the H-bridge circuit module. Output signal of the motor is connected to the VR Sink module which feeds back position and direction information of the massage robot in VR to guide the massage robot.

Four infrared sensors were used to detect the edge to avoid fall off the back, and another four infrared sensors were used to avoid collision and obstacles. The layout of the sensors was shown in Figure 1(a), while the hardware design scheme of the control system is described in Figure 9.

Simulation results

In the previous work, the tapping path of the massage robot was analyzed with the boustrophedon path planning algorithm and improved the boustrophedon path planning algorithm; the massage path of the massage robot was simulated and the massage area coverage of these two path planning algorithms was calculated. The coverage that is calculated from coverage = overriding raster/all raster is used as a significant index to evaluate the efficiency of path planning algorithm. From the calculation, the regional coverage of the boustrophedon path planning algorithm is 35.27%, while the coverage of the improved algorithm increases to 60.27%, which indicates the performance gets improved with the proposed algorithm. However, the massage robot in this article could not be regarded as a particle relative to the environment. Therefore, for the special limited working environment, this article proposes an efficient full area coverage path planning algorithm based on grid mapping.

Considering the unreachable area of back margin, the improved boustrophedon path planning algorithm was

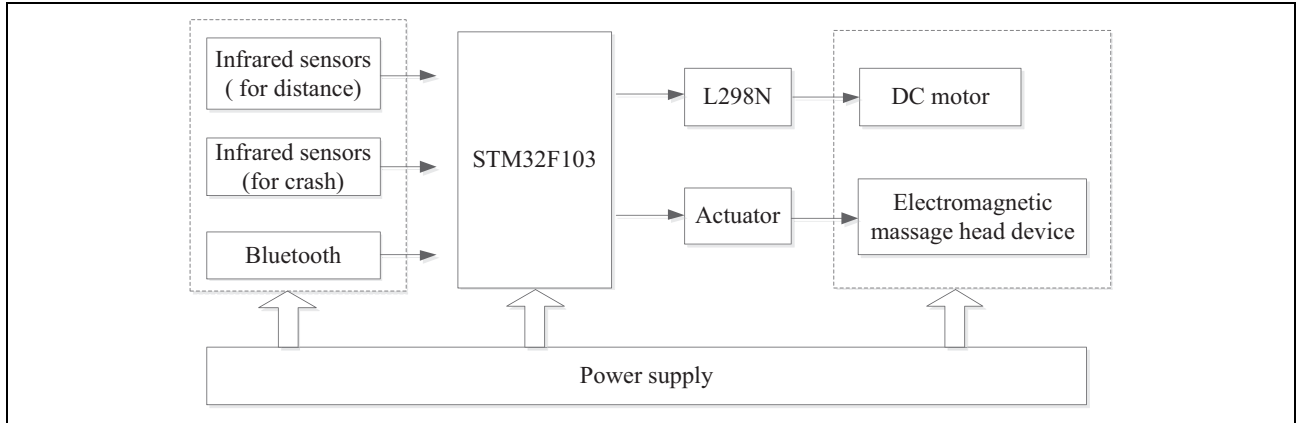


Figure 9. The hardware design scheme of the control system.

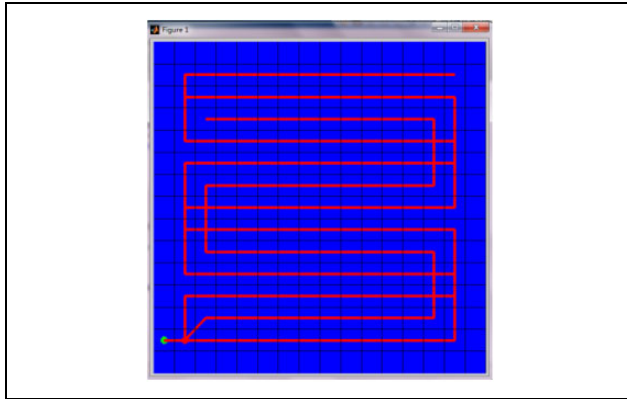


Figure 10. The results of improved boustrophedon path planning algorithm combined with BFS search algorithm. BFS: breadth-first search.

combined with BFS algorithm to investigate the coverage, and its simulation result is given in Figure 10. The blue area represents the unreachable area, and the calculated massage area coverage reaches up to 100%. Therefore, it can be concluded that the proposed efficient full coverage path planning algorithm is efficient for the designed robot in a limited environment, and no specific information of the environment is required in advance.

Experimental test

To evaluate the effectiveness of the presented massage robot and the proposed method, the massage effect test and path planning test were designed, respectively. Meanwhile, the possible effect factors were analyzed to improve the effectiveness by experimental tests.

Massage effect test and influence factors analysis

The acceleration values could be used to estimate massage effect with tapping operation as it indicates the interaction forces between human back and massage head, and also the influence of coil input voltage, signal duty cycle and back

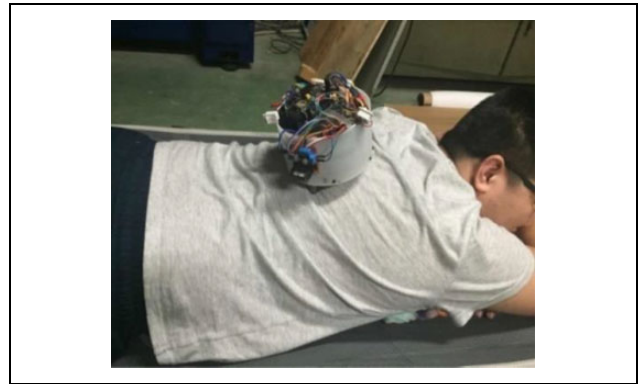


Figure 11. Motion test on human back.

elasticity on the massage effect was analyzed. The programmed motion tests were implemented on a volunteer's back (see Figure 11) based on the presented wheeled portable massage robot and test platform, and ADXL362 sensor was chosen to record acceleration values.

The duty cycle of the input signal, the voltage value of the input signal and flexibility of massage point were discussed to analyze the influence on massage effect and to help decide the optimal parameters.

Duty cycle of input signal

For this test, the experimental parameters and recorded acceleration values were listed in Table 3. The data were recorded from 5 s to 10 s, and the curves of the massage head acceleration changes with time at each duty cycle are drawn in Figure 12.

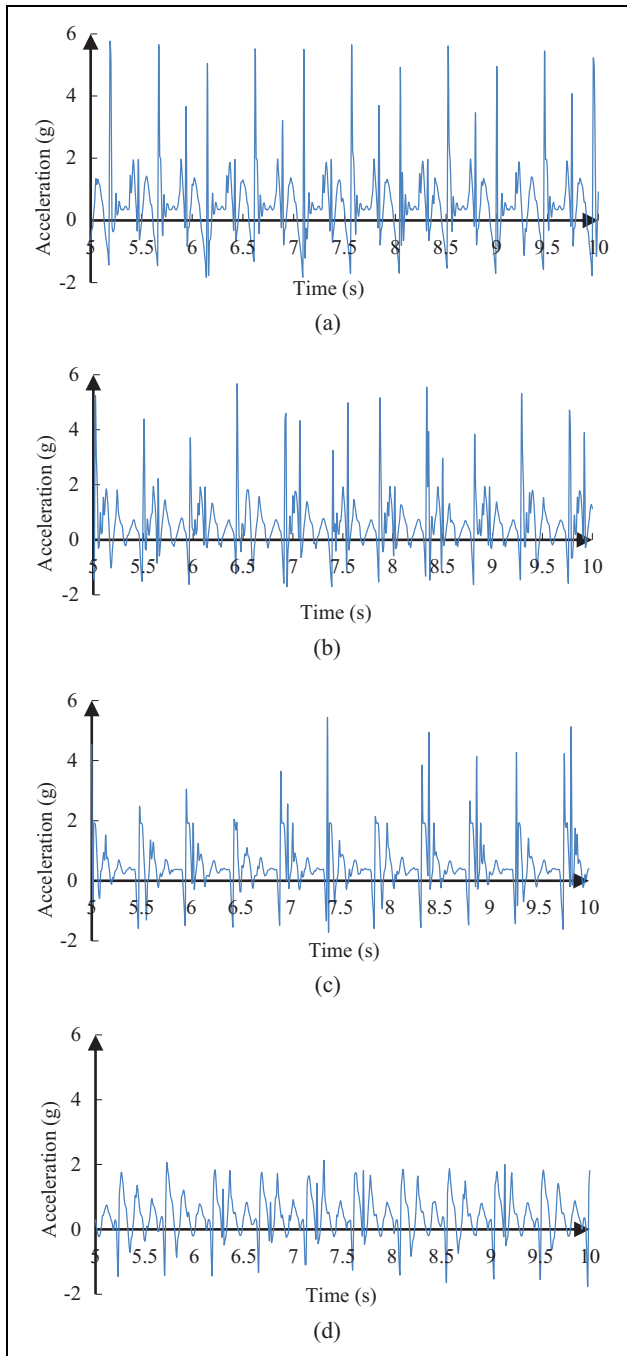
As mentioned in Figure 12, it indicates that with the increase of the duty cycle of the coil voltage (greater than 1/8), the acceleration amplitude keeps constant; when the duty cycle decreases, the acceleration decreases. As long as the massage head completes the entire massage, duty cycle basically has no effect on massage head acceleration. However, when the duty cycle is less than 1/8, the massage head is rebounded back, while all massage trip is not completed

Table 3. Experimental parameters and test results for duty cycle.

Voltage (V)	33			
Frequency (Hz)	2			
Sampling time (s)	20			
Duty cycle	1/16	1/8	1/4	1/2
Acceleration value (g)	2	5	6	6

Table 4. Experimental parameters and test results for voltage value.

Duty cycle	1/2		
Frequency (Hz)	5		
Sampling time (s)	20		
Voltage value (V)	25	29	33
Acceleration value (g)	4.7	5.6	6.6

**Figure 12.** Curves of acceleration at different duty cycles. (a) Duty cycle 1/2. (b) Duty cycle 1/4. (c) Duty cycle 1/8. (d) Duty cycle 1/16.

yet, and the distance from the moving core to the yoke at this time is large, which caused the electromagnetic force and the acceleration value to be small. The acceleration value is proportional to massage force and massage effect. Thus, when the duty cycle is in the range of 1/8–1/2, the massage effect is comparatively obvious than 1/16.

Voltage value of the input signal

The experiment parameters and recorded values were listed in Table 4, and the recorded acceleration curves are shown in Figure 13. It demonstrates that when the frequency and duty cycle of the input signal are determined, the acceleration amplitude increases with the increase of the input voltage. It means that the electromagnetic force increases with the input voltage value, which is consistent with the simulation results. As a result, the simulation method is proven to be feasible.

Flexibility of massage area

The experimental analysis of massage effect caused by duty cycle and voltage value was obtained under no-load condition. This section measures the acceleration values with load. When the elasticity of the human back tissue layer is less, the resistance for the massaging head to produce is greater. When the massage frequency is 5 Hz, duty cycle is 1/2, coil input voltage is 33 V and three kinds of states, completely relaxed, tight and extremely tight, on behalf of different levels of hardness of the back. The experimental data of the above setting were recorded (see Figure 14), and the acceleration amplitudes in the three states are 4.2, 5.2 and 5.6 g, respectively.

Comparing the results shown in Figures 12 to 14, it indicates that the acceleration value is less with load condition than no-load due to the back resistance of the human body. Meanwhile, the acceleration signal amplitude of the massage head gradually increases as the back gets harder. The reason is that the resistance of the back soft tissue gradually reduces with the change of the back hardness. Therefore, to improve massage effect, the user should get relaxed as much as possible to avoid fierce beat from the massage head.

Path planning test and analysis

In order to verify the feasibility of the proposed efficient full coverage path planning algorithm and the accuracy of robot motion control, a test platform was built for the

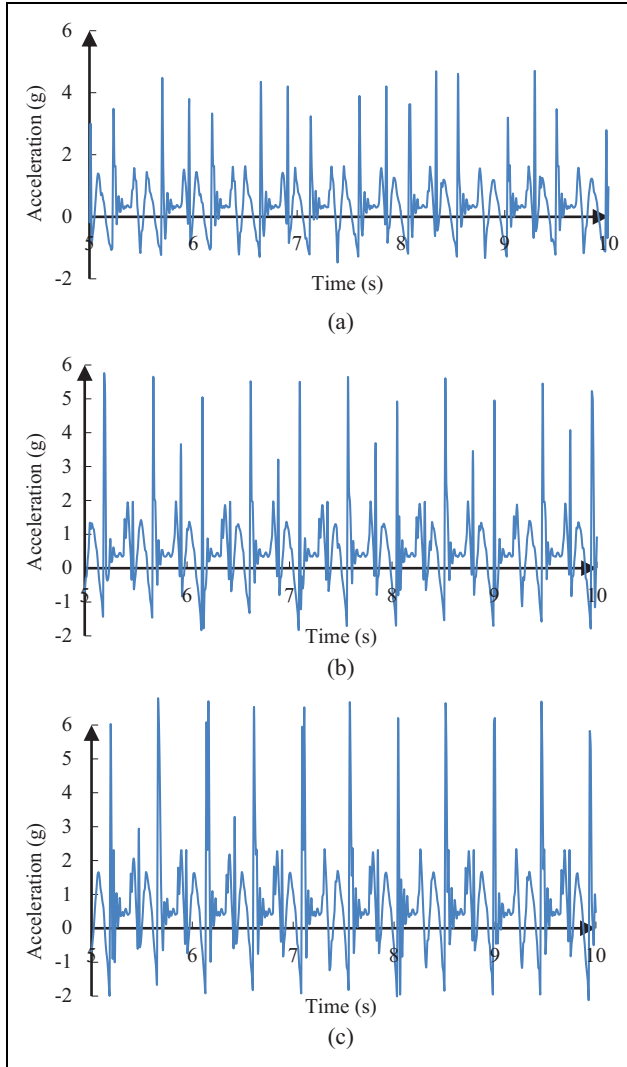


Figure 13. Curves of acceleration with different input voltages. (a) 25 V. (b) 29 V. (c) 33 V.

designed massage robot (see Figure 15(a)). The experiments were carried out on the limited planned area of the desktop (see Figure 15(b)) where the massage robot walks along the marked red line. The edge obstacles and cliffs were used to imitate the back environment of the human body. It can test whether the massage robot walks along the planned path, or exactly predicts the edge and cliff, and eventually calculates the coverage.

For the path planning experiments, when the robot went to the unexpected path, it was judged as failure. In the first group of experiments, tests were carried out 30 times, and 12 times failed, so the success rate was 60%. To summarize the reasons that caused the failure, the possible problems are listed as follows:

- 1) The robot could not turn 90° , which was designed in the programme.
- 2) There was motion deviation when the robot linearly moved.

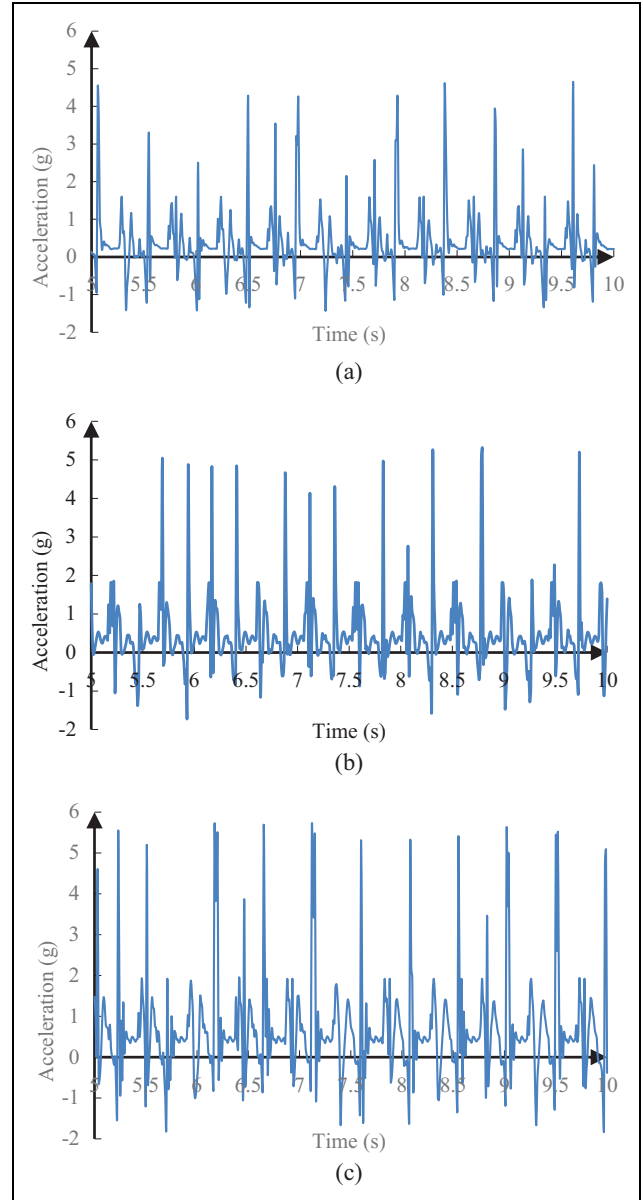


Figure 14. The curve of acceleration in different massage states. (a) Completely relaxed. (b) Tight. (c) Extremely tight.

- 3) The robot did not cover the edge area of the planned route.
- 4) The endless loop occurred when the robot ran into the corner of the expected environment.

To solve the above-mentioned problems and improve the performance of the massage robot and algorithm, the following measures were seriously implemented for the preparation of the next group of experiments. For the deformation of the wheels, they were polished and re-fabricated to make the structure rigidly symmetric. One more layer of rubber was added to the wheels to increase friction and reduce the lag during moving massage. The edge was not entirely covered as the unreasonable fixture of distance sensors. Therefore, the distance was repeatedly adjusted

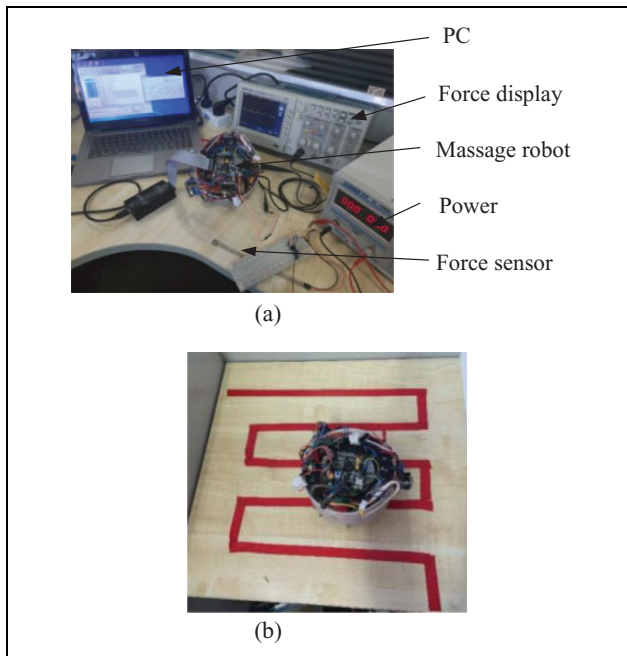


Figure 15. Test platform and path planning environment. (a) Test platform. (b) Path planning results.

to reduce the uncovered area of the edge. Meanwhile, the dead angle and endless loop were resolved by optimizing programming.

With the above-mentioned improvement, another group of experiments was carried out 30 times again. Then, it succeeded 26 times and failed 4 times. Consequently, the success rate is improved to 86.7% from 60% which basically achieved the desired results.

Conclusions

Currently, massage robots have become one of the important research studies focusing on the increasing requirements of healthcare. A space-saving and compact massage robot that provides three kinds of massage operation was designed for limited human back environment. Based on the principle of electromagnetic induction, the massage head was designed to achieve tapping massage. The rolling and kneading massage operations were achieved by specific roller design and motion programming. The 3D model of the massage head was established in Maxwell for force simulation. The influence of the coil voltage, the coil turns and the distance between the moving core and the yoke on the electromagnetic force was analyzed by orthogonal test, and the magnetic induction B and the winding distribution vector were obtained. The electromagnetic simulation results show that the coil voltage of the massage head is more sensitive to the electromagnetic force of the moving core compared to other factors.

An efficient full coverage path planning algorithm was designed combining with BFS algorithm. The path planning simulation results show that the proposed algorithm

reduced unreachable area and improved massage coverage without requiring environment model. The presented portable massage robot and control system was fabricated to verify feasibility, and the tests were performed on a volunteer's back. Furthermore, the duty cycle of input signal, the voltage value of input signal and flexibility of massage area were discussed to optimize the massage effect by measuring the acceleration values. Extensive path planning experiments show that the proposed path planning algorithm is proven to effectively improve the massage coverage and also promote the massage effect.


Declaration of conflicting interests

The author(s) declared no potential conflicts of interest with respect to the research, authorship, and/or publication of this article.

Funding

The author(s) disclosed receipt of the following financial support for the research, authorship, and/or publication of this article: This work was supported by the National Natural Science Foundation of China (grant no 51605385), the Natural Science Foundation of Shaanxi Province (grant no 2017JQ5026) and Fundamental Research Funds for the Central Universities (grant no 3102017zy008).

ORCID iD

Wendong Wang  <http://orcid.org/0000-0002-2336-0477>

References

1. Fazeli MS, Pourrahmat MM, Liu M, et al. The effect of head massage on the regulation of the cardiac autonomic nervous system: a pilot randomized crossover trial. *J Altern Complement Med* 2016; 22(1): 75–80.
2. Guo B, Han J, Li X, et al. Research and design of a new horizontal lower limb rehabilitation training robot. *Int J Adv Robot Syst* 2016; 13(1): 1–10.
3. Cheatham SW and Kolber MJ. Does roller massage with a foam roll change pressure pain threshold of the ipsilateral lower extremity antagonist and contralateral muscle groups? An exploratory study. *J Sport Rehabil* 2018; 27(2): 165–169.
4. Wang ZL, Liang Q, and Zhang BC. Structural design of the robot arm for massage based on the chain drive. *Adv Des Res Manuf Pts 1-3* 2013; 605–607: 1547–1551.
5. Su CZ, Shao FC, Liu J, et al. Measuring geometrical parameters of non-standard involute spur gears for humanoid massage robot with reverse solution. In: *IEEE international conference on robotics and biomimetics (Robio)*, Zhuhai, China, 2015, pp. 847–852. IEEE.
6. Li SH and Hao CZ. The development of the humanoid massage robot controller. In: *international conference on control engineering and automation (Iccea 2014)*, Chongqing, China, 2014, pp. 54–57. Destech Publicat Inc.
7. Hu N, Li CS, Wang LF, et al. Intelligent monitoring-based safety system of massage robot. *J Cent South Univ* 2016; 23(10): 2647–2658.

8. Huang Y, Li J, Huang Q, et al. Anthropomorphic robotic arm with integrated elastic joints for TCM remedial massage. *Robotica* 2015; 33(2): 348–365.
9. Ishii H, Koga H, Obokawa Y, et al. Path generator control system and virtual compliance calculator for maxillofacial massage robots. *Int J Comput Assist Radiol Surg* 2010; 5(1): 77–84.
10. Luo RC and Hsieh KC (eds). Tapping motion control of dynamic impulse-momentum contact to human body for robotic therapeutical percussive massage. In: *26th IEEE international symposium on industrial electronics, ISIE 2017*, 18 June 2017 – 21 June 2017. Edinburgh: Institute of Electrical and Electronics Engineers Inc.
11. Gao H, Lu S, Wang T, et al. Research and development of Chinese medical massage robot. *J Robot* 2011; 33(5): 553–562.
12. Arijji Y, Nakayama M, Nishiyama W, et al. Potential clinical application of masseter and temporal muscle massage treatment using an oral rehabilitation robot in temporomandibular disorder patients with myofascial pain. *Cranio* 2015; 33(4): 256–262.
13. Ishii H, Koga H, Obokawa Y, et al. Development and experimental evaluation of oral rehabilitation robot that provides maxillofacial massage to patients with oral disorders. *Int J Robot Res* 2009; 28(9): 1228–1239.
14. Sayapin SN (ed). Intelligence self-propelled planar parallel robot for sliding cupping-glass massage for back and chest. In: *1st international conference of artificial intelligence, medical engineering, and education, AIMEE 2017*, 21 August 2017 – 23 August 2017. Moscow: Springer Verlag.
15. Wei YZ, Gu KF, Cui XJ, et al. Strategies for feet massage robot to position the pelma acupoints with model predictive and real-time optimization. *Int J Control Autom* 2016; 14(2): 628–636.
16. Wang YC, Wu CY, and Chung PC. Constraint-based correspondence matching for stereo-based interactive robotic massage machine. *J Int Robot Syst* 2013; 72(2): 179–196.
17. Liu JS, Cheng JL, and Gong Y (eds). Study on optimal scheduling methods of urban drainage pumping stations based on orthogonal test. In: *2013 international conference on mechatronics, robotics and automation, ICMRA 2013*, 13 June 2013 – 14 June 2013. Guangzhou: Trans Tech Publications Ltd.
18. Wang WD, Zhang L, Li JZ, et al. The force control and path planning of electromagnetic induction-based massage robot. *Technol Health Care* 2017; 25: S275–S285.
19. Choi S, Lee S, Viet HH, et al. B-Theta*: an efficient online coverage algorithm for autonomous cleaning robots. *J Int Robot Syst* 2017; 87(2): 265–290.
20. Khan A, Noreen I, Ryu H, et al. Online complete coverage path planning using two-way proximity search. *Int Serv Robot* 2017; 10(3): 229–240.
21. Wang WD, Zhang P, Shi YK, et al. Design and compatibility evaluation of magnetic resonance imaging-guided needle insertion system. *J Med Image Health Inform* 2015; 5(8): 1963–1967.
22. Meera CS, Sairam PS, and Gupta MK. Path planning and motion control for a 3 DOF massaging robot. In: *International conference on robotics and automation for humanitarian applications (Raha)*, Kerala, India, 2016, pp. 42–47. IEEE.
23. Batsaikhan D, Janchiv A, and Lee SG. Sensor-based incremental boustrophedon decomposition for coverage path planning of a mobile robot. *Adv Int Syst* 2013; 193: 621–628.
24. Ryu H and Chung WK. Local map-based exploration using a breadth-first search algorithm for mobile robots. *Int J Prec Eng Man* 2015; 16(10): 2073–2080.